Molecular Crystals and Liquid Crystals Science and Technology. Section A. Molecular Crystals and Liquid Crystals

Publication details, including instructions for authors and subscription information:
http://www.tandfonline.com/loi/gmcl19

Kink Propagation in Freely Suspended SmC* Films

R. Stannarius [a] & C. Langer [a]

[a] Universität Leipzig, Fakultät für Physik und Geowissenschaften Linnéstrasse 5, D-04103, Leipzig

Version of record first published: 24 Sep 2006

To cite this article: R. Stannarius & C. Langer (2001): Kink Propagation in Freely Suspended SmC* Films, Molecular Crystals and Liquid Crystals Science and Technology. Section A. Molecular Crystals and Liquid Crystals, 358:1, 109-123

To link to this article: http://dx.doi.org/10.1080/10587250108028275

Mol. Cryst. and Liq. Cryst., 2001, Vol. 358, pp. 109-123
Reprints available directly from the publisher
Photocopying permitted by license only

Kink Propagation in Freely Suspended SmC* Films

R. STANNARIUS and C. LANGER

Universität Leipzig, Fakultät für Physik und Geowissenschaften Linnéstrasse 5, D-04103 Leipzig

We present numerical simulations of ferroelectric switching in freely suspended smectic films. Travelling 180° walls (kinks) in the film plane are quantitatively analyzed. Conditions for the formation of such walls are discussed. In addition to the conventional viscous and elastic torques and electric coupling terms to the external field, our model considers the polarization charges in the walls. The ferroelectric material interacts with the electric field produced by these charges, and the model allows for a partial screening of this field by free ionic charge carriers in the smectic film. The results of the numerical calculations are compared with electro-optic experiments performed with a polarizing microscope.

Keywords: Smectic films; Ferroelectric switching; Electro-optic effects; Kink propagation

INTRODUCTION

The formation of propagating wave fronts is a phenomenon often observed in systems which are suddenly quenched from equilibrium into an unstable state. A considerable number of theoretical studies has been devoted to the analysis of the static and dynamic properties of such structures. The concept of marginal stability has been developed to describe the selection of the propagation velocity [1, 2, 3]. Liquid crystals exposed to electromagnetic fields represent an experimental system where the properties of such structures can be conveniently studied. Different types of inversion walls have been described for example in nematic liquid crystals under the influence of magnetic (e.g. [4, 5, 6, 7, 8]) and electric fields (e.g. [9, 10]). These walls can represent stationary structures between equivalent states, but they propagate when the symmetry is broken for example by oblique external fields [4] or for non-symmetric wall profiles (Bloch walls [6, 8]).

In smectic C and C^* materials, similar kink structures have been predicted for the c-director, the projection of the molecular tilt direction on

the smectic layer plane. Schiller et al. [13] have given the first theoretical description of inversion walls in smectic C material in sandwich cells under the influence of electric fields. In weakly ferroelectric material, the spontaneous polarization provides the symmetry breaking element and travelling walls are formed. The dynamic equations for the c-director have the form of overdamped sine-Gordon equations, which are well known for their kink solutions. In the geometry of sandwich cells, the direct investigation of such structures is not easy. Inversion walls parallel to the electrode planes are not easily detectable by optical means, and their description requires assumptions about the director profile along the cell normal. Freely suspended films of smectic C and smectic C* materials provide a convenient alternative to study the electro-optic switching processes. When an electric field is applied in the film plane, the characteristics of the film reflectivity can be easily exploited to evaluate switching times and viscous parameters [11, 12]. Since the smectic layers are stacked perfectly in the plane of the film, the geometry of the experiment with in-plane electric fields is largely simplified. It has been recognized earlier that the reorientation of the c-director in an external electric field is not necessarily uniform in the film plane but can occur in the form of domain growth together with the appearance of localized travelling walls [14, 15, 16]. Spatially resolved images obtained with polarizing microscopy allow the direct observation of these inhomogeneous switching processes.

In this paper we analyze the switching mechanism of ferroelectric SmC* films in lateral electric fields. We explore the conditions for uniform switching and for the formation of kinks during the director reorientation in the external electric field. The key parameters of the model, in addition to viscoelastic properties of the smectic material, are the spontaneous polarization and electric conductivity of the sample. We use the results of numerical simulations to interpret experimental observations.

EXPERIMENT

The experimental geometry where kink switching has been observed before [16] is depicted in Fig. 1. The freely suspended film is drawn on a frame consisting of two fixed and two movable holders. The film area is approximately 6×6 mm A homogeneous electric field in the layer plane is generated by two plate electrodes forming a capacitor of 0.5 mm gap and 2.5 mm width. These electrodes are carefully pierced through the film from below. This technique allows to keep the film meniscus at the electrode surfaces very small. The maximum voltage in the experiments was 120 V, typically the electric fields applied were of the order of 10^4 to 10^5 V/m. The reflection images were observed with a polarizing microscope (NU-2, *Carl-Zeiss Jena*) and recorded by means of a CCD camera. A *HAMAMATSU* controller C2400 was used for contrast enhancement before the images were digitized.

The mesogenic material investigated was *ZLI 4237-100* from *Merck*

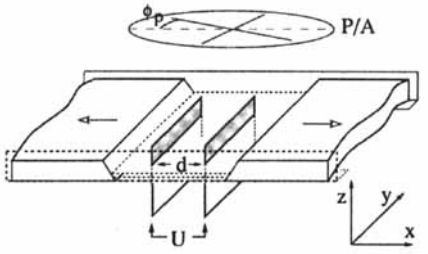

Figure 1: Drawing of the film holder with micro electrodes pierced into the film. Polarizer and analyzer orientations are sketched at the top.

with a SmC* phase at room temperatures, a spontaneous polarization $P_S = 2 \cdot 10^{-4} As/m^2$, rotational viscosity of the c-director $\gamma = 0.185 Pa\,s$ and tilt angle $\theta = 24.5°$ (at 20°C). The conductivity of the material is $1.3 \cdot 10^{-9} \Omega^{-1} m^{-1}$, it may differ somewhat for the individual samples, the dielectric constant is $\approx 3.5..4.5$.

OBSERVATIONS

In a sufficiently strong DC electric field, the sample aligns with the polarization $\vec{P}_S$ along the electric field (x-axis), and the c-director along y. The film becomes practically monodomain. For the material parameters of the investigated compounds, the critical electric field nessary for the unwinding of the SmC* helix is of the order of only 1 kV/m, therefore the helix is unwound for all voltages applied, even for films which are not thin compared to the helical pitch.

After switching the polarity of the electric voltage at the electrodes, the c-director field is in an unstable equilibrium and it reorients by 180° into the new equilibrium orientation. This can occur in different ways. The simplest case is a uniform rotation of the c-director in the film plane. This case is usually observed in thin films (thickness $s \ll 1\mu m$). In thicker films, we observe the formation of inversion walls near the lateral electrode plates. They start to propagate towards the opposite electrode, practically without changing their shapes. These structures obviously provide a classical example for front propagation into an unstable state.

Figure 2a shows an instant image of the free-standing film taken at a low electric field (60 kV/m) shortly after the field reversal. At each electrode a kink is released that propagates towards the middle of the film plane. These structures have been described in more detail in a previous publication [16]. The optical appearance of the film is quite similar behind and in front of the kink. The corresponding domains, which obviously differ in their c-director orientations by 180°, are optically indistinguishable at normal incidence. We assume that the film reflectivity I is related to the director orientation (in absence of twist) by

$$I(\varphi) \propto \sin^2 2(\varphi - \varphi_0) \qquad (1)$$

where φ is the angle between c-director and y-axis (or between $\vec{P}_S$ and $\vec{E}$), and φ_0 denotes the angle between the polarizer and the x-axis. This approximation holds when the c-director field is uniform along the film normal (z-axis) and if the variation of $\varphi(x, y)$ occurs on a scale that is large compared to the optical wavelength, such that plane waves can be assumed.

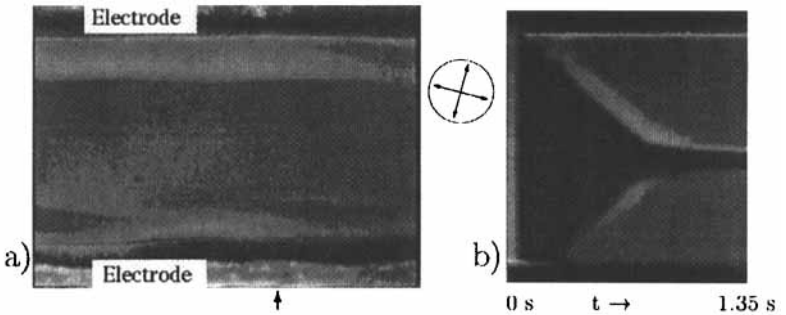

Figure 2: Experimental image of a 3.2 μm thick film of *ZLI 4237-100* after switching from -30 V to +30 V, electrodes are seen in the upper and lower edges of the picture (top view): (*a*) instant image 0.34 s after field reversal, (*b*) time evolution of a vertical cross section taken at the arrow position. In the circle between both images, the orientation of the polarizers is indicated.

The time evolution of the walls is shown in Fig. 2b in a spatio-temporal plot. This image was constructed from a sequence of cross sections of the images taken during the reorientation (perpendicular to the electrodes at the position indicated by the small arrow below Fig. 2a). Here one can see that the kinks move with the same constant velocity. In the middle of the film plane they interact with each other, forming a 360° wall. The propagation stops. The 360° wall is finally distorted and destroyed by electroconvective flow in the film or by defects moving in from the sides (because of the finite electrode width), but before this happens it can be seen from image 2b that a stationary state is reached.

We also note the change of brightness in a narrow stripe directly at the electrodes after the switching (Fig. 2b top and bottom). Initially, the bright edge is at the lower electrode, after the c-director reorientation it appears at the opposite electrode. The explanation is found from the model director field sketched in Fig. 3. At the film boundaries, the c-director tends to align perpendicular to the electrodes, so the optical intensity increases at one electrode where the c-director is deflected towards the diagonal between the polarizers, at the other edge the reflection image darkens because the c-director is deflected towards the polarizer. Immediately after field reversal, the polarization $\vec{P}_S$ is (except near the electrodes) antiparallel to the electric field, the electric torque is zero. The reorientation process in the film middle

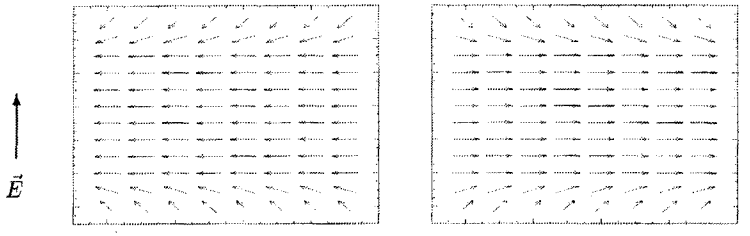

Figure 3: Schematic view of the c-director field in the film plane before and after switching. The spontaneous polarization $\vec{P}_S$ is perpendicular to the c-director in the film plane.

is therefore delayed and initiated only by director fluctuations. The 'pretilt' angle at the lateral film boundaries (irrespective of its physical origin, which will not be discussed here) initiates the ferroelectric switching there and leads to the formation of the inversion walls.

The velocity v of the wall motion increases roughly proportional to the external electric field with a mobility of $\mu = v/E \approx 4.2 \cdot 10^{-9} m^2 V^{-1} s^{-1}$. The width of the kinks is approximately proportional to E^{-1}. Because of the particular director configuration here, the reorientation at the two electrodes starts in opposite directions. The kinks always have opposite signs. When the two domains approach each other in the middle of the film plane, the two kinks merge to a 360° wall. The wall front is not exactly parallel to the electrodes. With increasing field strength, the kinks adopt more and more zig-zag shape [16]. An example is shown in Fig. 4. This particular feature is discussed below.

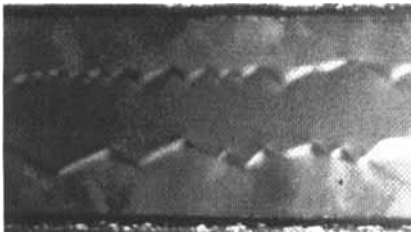

Figure 4: Zig-zag shaped kinks at E=120 kV/m.

MODEL

In this section we will propose a mechanism for the formation and propagation of inversion walls in ferroelectric smectic films. An exact description of the experimental structures would require a three-dimensional analysis of the director field dynamics. This will not be attempted here. Instead, we will present a simplified one-dimensional model which describes satisfacto-

rily the principal features of the kinks. In our model, we assume that the film is uniform along z, we neglect the twist term and use a one-constant approximation for elastic in-plane distortions of the c-director field. The dynamic equation for the reorientation of φ contains four terms.

$$\gamma\dot{\varphi} = -P_S E \sin\varphi + \epsilon_a\epsilon_0 E^2 \sin\varphi\cos\varphi + K\Delta\varphi \qquad (2)$$

(viscous) (ferroelectric) (dielectric) (elastic)

In the high P_S ($> 10nC/m^2$) materials studied here, and for the electric fields used in our experiments, the dielectric term is at least two orders of magnitude smaller than the ferroelectric term in Eq. 2, it will further be neglected in the calculations. For the description of the in-plane uniform reorientation after electric field reversal, the elastic term can be dropped as well and Eq. [2] reduces to $\gamma\dot{\varphi} = -P_S E \sin\varphi$ which has the analytical solution

$$\tan\frac{\varphi(t)}{2} = \tan\frac{\varphi(0)}{2}\exp(-\omega_0 t) \quad \text{with} \quad \omega_0 = \frac{P_S E}{\gamma} \qquad (3)$$

For the spatially non-uniform solutions of Eq. 3 we will first assume that the electric field is uniform in the film plane. With the substitutions

$$t' = \omega_0 t = \frac{P_S E}{\gamma} t \qquad x' = \frac{x}{\xi} = \sqrt{\frac{P_S E}{K}}\, x$$

one obtains the dimensionless equation

$$\frac{\partial\varphi}{\partial t'} = -\sin\varphi + \varphi_{x'x'} \qquad (4)$$

Solutions of this type of equation have been comprehensively investigated both analytically and numerically [18, 17, 19, 20]. Between two boundaries with antiparallel c-director orientation, it has been shown that a kink solution exists. It is depicted in Fig. 5. Its dimensionless velocity is $v' = 2$ which corresponds to an actual kink velocity $v = 2\sqrt{P_S E K}/\gamma$ [17, 19].

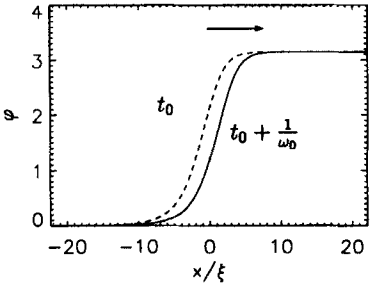

Figure 5: Kink solution of Eq. 4, the wall moves into the unstable region (right). The spatial coordinate is scaled with $\xi = \sqrt{K/(P_S E)}$. Propagation velocity, width and shape of this type of kinks are not in accordance with the experimental structure shown in Fig. 2.

However, this model is correct only in very thin films where the con-

tributions of the polarization charges in the wall can be neglected. These charges appear as a consequence of the rotation of $\vec{P}_S$ across the inversion wall. They contribute to a considerable amount to the local electric field, and one has to take into account that the electric field term in Eq. 2 consists of the contribution of the external electric field plus the electric field created by polarization charges and free charge carriers in the film. Qualitative considerations lead to the following predictions: Because of the repulsive interactions of two adjacent domains with head-on orientations of the spontaneous polarizations, the inversion wall between them is broadened. The additional electric field adds to the external electric field in front of the wall (towards the anti-aligned domain) and it reduces the external field in the rear of the wall. This creates an asymmetric wall profile, the front edge will be much steeper than the rear part. Furthermore, the additional electric field will speed up the front propagation. Since the liquid crystalline material contains free ionic charge carriers, the polarization charges will be screened at least partially by these free charges which will be accumulated in the wall. However, even if enough charge carriers are present in the film, the mobility of the wall is by about one order of magnitude larger than that of the ions, therefore this screening will be incomplete.

The long-range influences of the polarization and free charges make an exact solution of the director equations very complicated. We solve the dynamic equations for c-director and charge fields using a numerical procedure. Some simplifying assumptions are made: We consider the one-dimensional geometry of a wall parallel to the electrodes which is finitely extended along y. The film is assumed to be uniform normal to the plane.

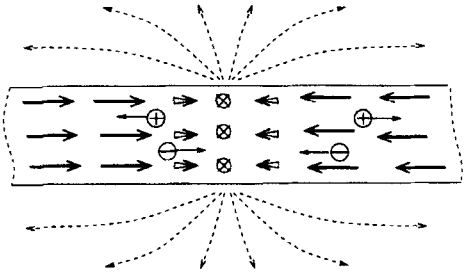

Figure 6: Schematic side view of the inversion wall (cross section of the film in the xz plane). Thick arrows indicate the spontaneous polarization, dotted lines visualize the electric field, the motion of ionic charges is indicated.

The polarization charge density is given by $\rho_p = -\vec{\nabla}\vec{P}_S$, in the 1D model it is related to φ by

$$\rho_p = P_S \sin\varphi \frac{\partial\varphi}{\partial x}. \tag{5}$$

The electric field of an infinitesimal line charge $\rho(x')\,dx'\,dz'$ at (x', z') is

$$dE_x(x,z) = \frac{\rho(x')}{2\epsilon\epsilon_0} \frac{(x-x')}{(x-x')^2 + (z-z')^2}\,dx'\,dz'$$

where we consider only the x component. The component dE_z of the electric field normal to the film plane is irrelevant for the c-director dynamics. Now we integrate over the normal coordinate z of the film (thickness s) to obtain the field of a slice dx' with charge density ρ. This approximation should be justified when the wall profile is very broad compared to the film thickness, it yields the total electric field

$$E(x) = E_0 + \int \frac{\rho(x')}{\pi\epsilon\epsilon_0} \arctan \frac{s}{2(x-x')}\, dx' \tag{6}$$

The electric current density j_x in the film is given by Ohm's law

$$j_x = \sigma E, \tag{7}$$

and the accumulation of free charges is described by the continuity equation

$$\dot{\rho}_f = \frac{dj_x}{dx}, \tag{8}$$

the charge density ρ is the sum of ρ_f and ρ_p.

In the numeric calculations, we start with an arbitrary initial profile $\varphi(x)$ of the 180° wall. The polarization charges and their electric field are calculated from the c-director profile by means of Eqs. 5, 6. The electric field determined from Eq. 6 is entered into the discretized Eq. 2 to calculate the director reorientation in the next time step and into Eqs. 7, 8 to calculate the change of the free charge distribution. Then the procedure is repeated in the next iteration step with the new electric field.

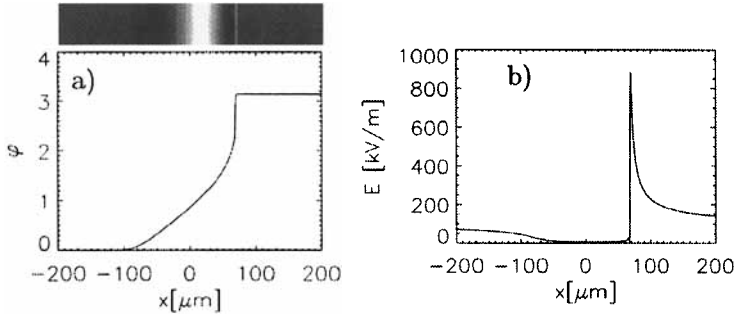

Figure 7: Calculated profile of the propagating inversion wall in a 3.2μm thick smectic film at E_0=100 kV/m external electric field, *a)* c-director orientation, *b)* local electric field strength. At the top the optical image calculated with Eq. 1 is shown for polarizers rotated by 15° with respect to the (x, y) frame; (parameters of *ZLI 4237-100*, see text).

The numerical approach uses a 1000 point discretization along x. We

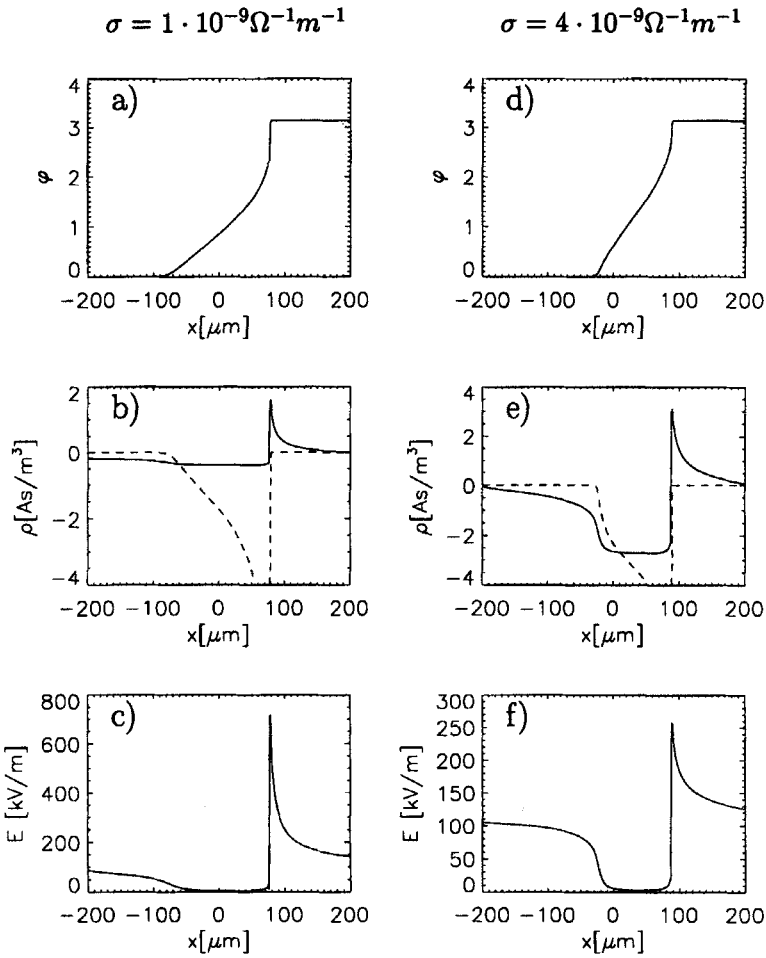

Figure 8: Calculated conductivity dependence of the c-director profile $\varphi(x)$ across the inversion wall *(a,d)*, the charge densities *(b,e)* and the electric field *(c,f)*, E_0=100 kV/m. The solid lines in graphs *(c,d)* represent the free charges ρ_f, the dashed lines indicate $-\rho_p$. Graphs *(a-c)* correspond to a low conductivity of $\sigma = 10^{-9}\Omega^{-1}m^{-1}$, *(d-f)* belong to $\sigma = 4 \cdot 10^{-9}\Omega^{-1}m^{-1}$.

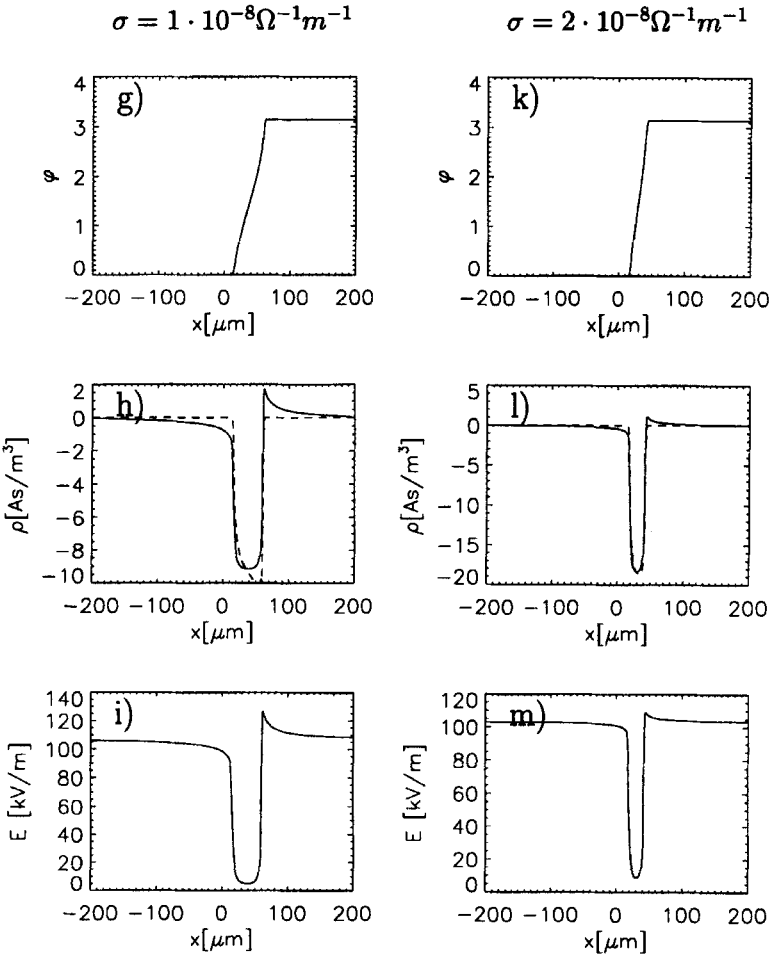

Fig. 8 continued: Graphs to the left *(g-i)* correspond to conductivity $\sigma = 10^{-8}\Omega^{-1}m^{-1}$, graphs on the right hand side *(k-m)* represent a highly conducting sample with $\sigma = 2 \cdot 10^{-8}\Omega^{-1}m^{-1}$. In the latter, the polarization charges are almost completely compensated by the free ionic charges, except for a slight lateral shift of the charge density curves because of the wall motion.

repeat the calculation cycle until the wall profile and charge distribution profile reach a stationary shape. Since the structure moves with velocity v along the spatial coordinate, the coordinate system is shifted continuously with the wall motion such that the kink remains in the middle of the discretized x range during the calculations. A typical simulated wall profile for a non-conducting high P_S film is shown in Fig. 7. An external electric field strength of 100 kV/m and a film thickness of 3.2 μm are assumed. Parameters have been taken from *ZLI 4237-100* where available. In addition to the quantities listed above, we have assumed an elastic constant K=3 pN. The choice of K influences the propagation velocity since it determines the steepness of the kink front, however, its influence on the tail and the total kink width is marginal.

It is obvious from Fig. 7 that the wall profile is considerably broader than the structure calculated without the self-energy contributions (Fig. 5) and the electric field is considerably changed near the kink. The effect of ionic charges is seen in the images of Fig. 8. The c-director profiles, charge densities and electric field distribution are collected for different conductivities of the smectic material. In Figs. 8a-c, a low conductivity sample is shown where the polarization charges are almost uncompensated, the wall profile is nearly similar to the non-conducting case. In Figs. 8d-f, the increasing compensation of the polarization charges is visible. It is accompanied by a narrowing of the kink and a decrease of the extra electric field. Inside the wall, the external field is almost completely shielded. The conductivity of the material used in the experiments ($\approx 1.3 \cdot 10^{-9} \Omega^{-1} m^{-1}$) is probably just in the range where its influence on the wall properties becomes noticeable, but the compensation of polarization charges is still rather small.

With a further change of the conductivity by only a factor of 2.5, the free charge density is almost sufficient to compensate the polarization charges. Figs. 8k-m show the highly conducting case where the free charges are of equal strength (and opposite sign) as the polarization charges. The field of the polarization charges outside the wall is compensated completely. Since the wall moves towards the energetically unstable domain, the charge densities ρ_p and ρ_f are slightly shifted with respect to each other. Therefore, the electric field inside the wall is very small, the external field is screened. In the external electric field outside the wall, the charges move until they reach the wall front, there they are accumulated and stop (in the low electric field in the wall) until the wall has passed.

Not only the shape and width of the walls is determined by the concentration and mobility of free charges in the film, but also the propagation speed is significantly influenced. Figure 9 shows the σ-dependence of the propagation speed and the wall width. The definition of an absolute wall width is of course somewhat subjective, we give here the range between $\varphi = 0.1\pi$ and 0.9π. Interesting for a quantitative comparison with the experiments is the field strength dependence of wall widths and velocities. These characteristics are presented in Fig. 10. Dashed lines indicate the ex-

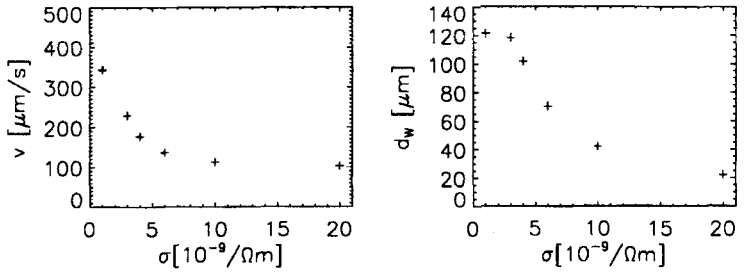

Figure 9: Calculated σ-dependence of the kink velocity v and width d_w (see text), $E_0 = 100kV/m$, other parameters as in Fig. 8.

perimental results from [16]. Both velocities and widths of the calculated structures have the same order of magnitude as in the experiment. The field strength dependence of the velocities is not in good agreement with the measurements. A comparison of Fig. 7 (top) with the images in Figs. 2a,b also shows that the overall optical profile is not well reproduced and in particular, the narrow bright line is not resolved in the experiment. Consequently, there is some subjectivity in the comparison of absolute wall widths.

Of course, also the experimental zig-zag shape is not considered by our one-dimensional model. In view of the crude approximations of the model, however, the basic properties of the experimental structures are satisfactorily reproduced.

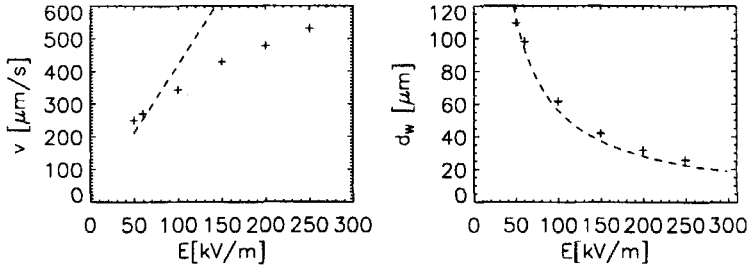

Figure 10: Calculated electric field dependence of the kink velocity v and kink width d_w (see text), a conductivity of $10^{-9}\Omega^{-1}m^{-1}$ is assumed.

DISCUSSION

The qualitative predictions given in the beginning of the previous section are confirmed by the calculations. In strongly ferroelectric smectic material the spontaneous polarization reversal in an inversion wall leads to self-energy contributions with characteristic effects on wall shapes and dynamic properties. The kink profiles are asymmetric, the tail of the kinks is very broad, the propagation velocity is much faster than that of kinks calculated without the self-energy terms.

The model can also explain why the kinks are observed in the experiment only in films thicker than about 1μm. The polarization charge density is given by the divergence of $\vec{P}_S$, and therefore the polarization charges per film area are directly proportional to the film thickness. In thin films, the additional field created by these charges is too weak to take effect, and the shape and dynamic properties of the kink solution are as shown in Fig. 5. This structure is considerably narrower, and most important, its velocity is nearly one order of magnitude slower than that of the kinks described in our model. If such kinks are formed during field reversal, they move too slowly to be observed. The uniform reorientation of the film takes place as a competing ferroelectric switching mechanism. Initiated by director fluctuations or interactions of the c-director with convective flow in the film plane, the unstable antiparallel state switches uniformly towards the stable parallel state before the kinks have noticeably moved.

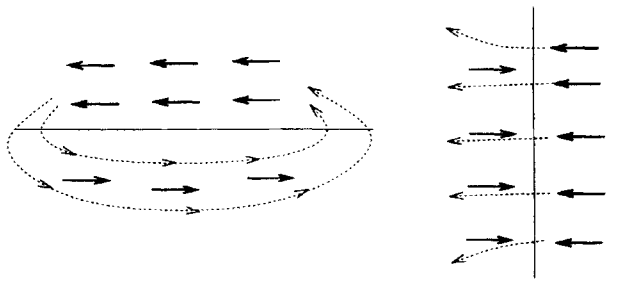

Figure 11: Two antiparallel domains with an inversion wall parallel *a)* and perpendicular *b)* to $\vec{P}_S$. Dotted lines symbolize the electric field created by one of the domains. The orientation *(a)* is energetically favourable.

Of course, we have neglected a number of important details. We have not considered the zig-zag deformation of the walls so far. This characteristic detail of the wall shape can presumably be interpreted as a static effect. Two domains with antiparallel orientations of the spontaneous polarization favour an orientation of the domain wall along the polarization directions, as is sketched in Fig. 11. The kinks formed at the electrodes, however, have the initially orientation *(b)*. A rotation of the wall lowers the interaction energy, but at the same time the arising zig-zag deflection of the wall increases

its length. Therefore, a compromise is adopted with a fixed equilibrium angle that depends upon the strength of the electric interactions of both domains. This strength, and consequently also the zig-zag angle, increases with decreasing wall width, and is therefore a continuous function of the external electric field. With increasing field strength E_0, the wall is quenched and the zig-zag angle increases [16]. This will also have consequences for the propagation properties, which have to be included in a refined dynamic model. Furthermore, we have neglected the spontaneous twist of the film completely. This is correct as long as the electric field strength is larger than the critical field for helix unwinding. It is obvious, however, from the graphs in Fig. 8, that the electric field inside the wall can be very low, and therefore we cannot exclude an additional c-director twist deformation there.

At last, we have not included the anisotropic properties of the dielectric tensor and film conductivity in the film plane. Also, the existence of surface charges has not been considered, and moreover all flow effects have been neglected, in particular the electroconvective flow which may be small but is always present in the free-standing films.

SUMMARY

We have simulated the formation of kinks during ferroelectric switching of freely suspended smectic films. The one-dimensional dynamical model allows for the electric field generated by polarization charges in the kink. This additional inhomogeneous electric field has dramatic influences on the shape and velocity of the kinks. With typical parameters of a commercial ferroelectric mixture, the propagation speed can increase up to one order of magnitude, the profile of the kink is very steep in the front, whereas it can be broadened considerably towards the tail. The ionic charges in the film can screen the polarization charges partially, thereby reducing the dramatic effects of the polarization charge field.

A comparison with experiments reveals a considerable similarity of the calculated patterns to structures observed in free-standing films during electro-optic switching experiments. We propose therefore that the model presented in this paper provides a sound basis for a qualitative and quantitative description of these experimental patterns, and to a general understanding of the role of polarization charges in ferroelectric smectics [21].

Acknowledgements

The authors acknowledge the DFG for financial support within the *Sonderforschungsbereich* 294 and grant *STA* 425/9.

References

[1] G. Dee and J. S. Langer; *Phys. Rev. Lett* **50** 383 (1983).
[2] E. Benjacob, H. Brand, G. Dee, L. Kramer, and J. S. Langer; *Physica D* **14** 348 (1985).
[3] W. van Saarloos; *Phys. Rev. A* **37** 211 (1988).
[4] F. Brochard; *J. Phys. (France)* **33** 607 (1972).
[5] Migler, K.B.; Meyer, R.B. *Phys. Rev. E* **48** 1218 (1993). Migler, K.B.; Meyer, R.B. *Physica D* **71** 412 (1994).
[6] Coullet, P.; Frisch, T.; Gilli, J.M.; Rica, S. *Chaos* **4** 485 (1994). Frisch, T.; Rica, S.; Coullet, P.; Gilli, J.M. *Phys. Rev. Lett.* **72** 1471 (1994). Frisch, T. *Physica D* **84** 601 (1995).
[7] Shagalov, A.G. *Phys. Lett. A* **199** 229 (1995).
[8] Nasuno, S.; Yoshimo, N.; Kai, S. *Phys. Rev. E* **51** 1598 (1995).
[9] A. Stieb, G. Baur, G. Meier ; *Ber. Bunsenges. Phys. Chem* **78** 899 (1979).
[10] H. Schmiedel, Ch. Cramer, R. Stannarius, K. Eidner, M. Grigutsch. *Liq. Cryst.,* **14** 1935, (1993). Ch. Cramer, U. Kühnau, H. Schmiedel, R. Stannarius. *Mol. Cryst. Liq. Cryst.* **257** 99, (1995).
[11] C. Escher, T. Geelhaar, and E. Böhm; *Liq. Cryst.* **3** 469 (1988).
[12] G. Hauck, H.D. Koswig, and C. Selbmann; *Liq. Cryst.* **21** 847 (1996).
[13] P. Schiller, G. Pelzl, and D. Demus, *Liq. Cryst.* **2** 21 (1987).
[14] S. Uto, H. Ohtsuki, M. Terayama, M. Ozaki, and K. Yoshino; *Jpn. J. Appl. Phys.* **35** L 158 (1996).
[15] C. Langer, and R. Stannarius, *Phys. Rev. E* **58** 650 (1998).
[16] C. Langer, and R. Stannarius, Proc. FLC99, subm. to *Ferroelectrics.*
[17] P. Cladis and W. van Saarloos; in *Solitons in Liquid Crystals,* L. Lam and J. Prost (eds), Springer-Verlag New York Berlin Heidelberg (1992).
[18] D. G. Aronson and H. F. Weinberger; *Adv. Math.* **30** 33 (1978).
[19] J. E. Maclennan, N. A. Clark, M. A. Handschy; in *Solitons in Liquid Crystals,* L. Lam and J. Prost (eds), Springer-Verlag New York Berlin Heidelberg (1992).
[20] I. W. Stewart; *IMA Journal of Appl. Math.* **61** 47 (1998). E. N. Tsoy, I. W. Stewart, F. Kh. Abdullaev; *Phys. rev. E* **60** in press (1999).
[21] Zhiming Zhuang, J. E. Maclennan, N. A. Clark; *Proc. SPIE* **1080** 110 (1989).